Int. J. Heat Mass Transfer. Vol. 33, No. 10, pp. 2191–2205, 1990
Printed in Great Britain

0017–9310/90 $3.00 + 0.00

Mass transfer by natural and forced convection in open cavities

CHEE BURM SHIN and DEMETRE J. ECONOMOU†
Department of Chemical Engineering, University of Houston,
Houston, TX 77204-4792, U.S.A.

(*Received* 11 *July* 1989 *and in final form* 11 *December* 1989)

Abstract—Time-dependent mass transfer by natural convection in two-dimensional open cavities is studied using the finite element method. Emphasis is placed on a system simulating selective chemical etching of thin solid films for microelectronic device fabrication. Time-dependent local and spatially-averaged Sherwood numbers are reported for a Schmidt number of 10^3, cavity aspect ratios (depth : width) of 1 : 4, 1 : 1, and 2 : 1, and for Rayleigh numbers of up to 10^5. The flow and concentration fields are symmetric at early times. However, symmetry breaking and oscillatory flows occur at later times. The formation of plumes result in effective communication between the external 'fresh' etching solution and the 'contaminated' solution within the cavity, especially for deep cavities which are otherwise difficult to access. Forced convection mass transfer is also studied for Peclet numbers of up to 10^4. When compared to forced convection, natural convection resulted in one order of magnitude better mass transfer in a 2 : 1 cavity. The results have important implications for deep anisotropic etching of thin solid films and other related processes.

1. INTRODUCTION

NATURAL convection in cavities is encountered in a variety of engineering problems and has received considerable attention in the literature [1]. In particular, natural convection in closed cavities has been studied extensively both theoretically and experimentally [2–4]. However, natural convection in open cavities or partial enclosures has received much less attention [5, 6]. This may be due to the complex interaction between internal flows and external conditions. In contrast, forced convection heat or mass transfer in open cavities has been studied to a great extent [7, 8]. The focus of the present work is an application of mass transfer by natural and forced convection in the manufacture of microelectronic devices.

Wet chemical etching of thin solid films using a photoresist mask (Fig. 1) is widely employed in the microelectronics industry [9]. Examples include etching of GaAs used in the fabrication of optoelectronic devices [10], and etching of copper films used in the fabrication of printed circuit boards. A common characteristic of the above and other similar processes is that the reaction rate and its distribution along the etching surface depend in a complex manner on the interaction among fluid flow, mass and heat transfer, and chemical reaction kinetics. In addition, the reaction rate depends on the instantaneous shape of the topographical feature or cavity, which in turn affects the further shape evolution of the cavity. The following discussion focuses on etching, although similar principles and methods of analysis apply to related processes such as electrodeposition through masks [11], and even localized corrosion [12].

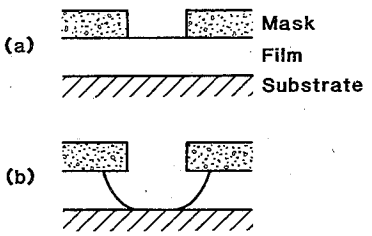

FIG. 1. Schematic of selective etching of a thin film through a resist mask : (a) before etching ; (b) after etching.

Important goals of the etching process are high etching rate, and low mask undercut (anisotropic etching). The process is often limited by mass transfer of the etchant from the solution bulk to the surface, or removal of the reaction product from the vicinity of the surface. Therefore, different methods have been used to enhance the mass transport, most noticeably impinging jet or cross flow over the cavity [8]. At the initial stages of the process, when the cavity is still shallow, such methods can be effective since the external flow can invade the cavity bringing 'fresh' solution into the cavity and washing the dissolution products away (Fig. 2(a)). As the cavity deepens, however, recirculating flow patterns develop within the cavity, and after a certain aspect ratio (depth : width) has been reached, the external flow can no longer penetrate the cavity [13]. In such a case, communication of the 'contaminated' solution trapped in the cavity with the external flow occurs only through a boundary layer along the cavity mouth (Fig. 2(b)). Since the recirculating eddy motion is weak, mass transfer and etching rate are drastically reduced. Further, the long etching times required result in excessive mask undercut. The situation becomes even worse when the cavity

† Author to whom correspondence should be addressed.

NOMENCLATURE

A	aspect ratio, $h/2L$	$\mathbf{U}$	dimensionless fluid velocity vector, $L\mathbf{u}/D$
c	species concentration [mol m^{-3}]	u_c	fluid velocity at center of cavity mouth [m s^{-1}]
c_∞	far-field species concentration [mol m^{-3}]	U_x	x-component of dimensionless fluid velocity
c_{sat}	species concentration at saturation [mol m^{-3}]	U_y	y-component of dimensionless fluid velocity
C	dimensionless species concentration, $(c-c_\infty)/(c_{sat}-c_\infty)$	x	horizontal spatial coordinate [m]
D	diffusivity [m^2 s^{-1}]	X	dimensionless horizontal spatial coordinate, x/L
h	cavity height [m]	y	vertical spatial coordinate [m]
$\mathbf{j}$	unit vector in the y-direction	Y	dimensionless vertical spatial coordinate, y/L.
k_x	local mass transfer coefficient [m s^{-1}]		
p	pressure [Pa]	Greek symbols	
P	dimensionless pressure, $(p-\rho_\infty \alpha y)L^2/(\mu D)$	α	gravitational acceleration [m s^{-2}]
Ra	Rayleigh number, $\alpha\beta(c_{sat}-c_\infty)L^3/(\nu D)$	β	coefficient of volume expansion [m^3 mol^{-1}]
Re	Reynolds number, $u_c L/\nu$	μ	viscosity [kg m^{-1} s^{-1}]
Sc	Schmidt number, ν/D	ν	kinematic viscosity [m^2 s^{-1}]
Sh_x	local Sherwood number, $k_x L/D$	ρ	density [kg m^{-3}]
Sh_{av}	average Sherwood number	ρ_∞	far-field density [kg m^{-3}].
t	time [s]		
T	dimensionless time		
$\mathbf{u}$	fluid velocity vector		

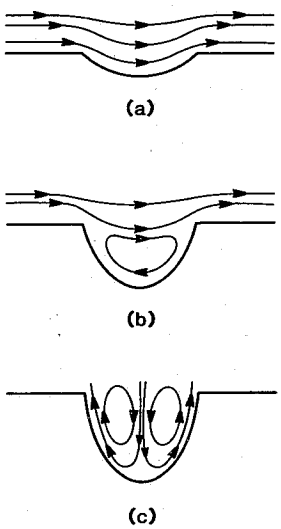

FIG. 2. Schematic of streamlines for flow over cavities. (a) Forced convection over a shallow cavity; external flow penetrates cavity resulting in good mass transfer. (b) Forced convection over a deep cavity; relatively slow recirculating flow reduces communication between outside solution and that inside cavity resulting in poor mass transfer. (c) Natural convection in deep cavity; communication between outside solution and that inside cavity is restored resulting in good mass transfer.

becomes deep enough for a second eddy to form underneath the first. The solution in this eddy is almost stagnant and transport is governed by diffusion.

A unique method to enhance mass transport in deep cavities makes use of density-gradient-induced natural convection [14]. In a typical etching situation, the solution density adjacent to the dissolving solid surface is different than in the bulk. Such density gradients can induce fluid motion by natural convection which can be further enhanced in an artificial gravity environment, e.g. by rotating the substrate. The natural convection flow patterns disrupt the mass transfer boundary layer which would otherwise exist along the cavity mouth. Fresh solution can now penetrate deep into the cavity and reaction products can be swept away (Fig. 2(c)), i.e. the communication between the external solution and that inside the cavity is greatly improved. The result is improved mass transfer rate and, if the process is mass transfer limited, improved etching rate.

Recently we developed a mathematical model to study the effect of mass transport and chemical reaction on the shape evolution of two-dimensional cavities undergoing etching [15]. The case of cross flow over the cavity in the absence of natural convection was considered. The purpose of the present investigation is to study the mass transfer enhancement in open cavities due to natural convection induced by density gradients during etching of a solid film. A fixed value of the Schmidt number $Sc = 1000$ was used which is typical of aqueous solutions. The effect of cavity aspect ratio and of Rayleigh number Ra was examined. Aspect ratios (depth : width) of 1 : 4, 1 : 1, and 2 : 1 were studied with Ra up to 10^5 (Ra was based on the cavity halfwidth). The results were compared to mass transfer due to forced convection alone in a

cross flow configuration with Peclet numbers $Pe = 10^2$, 10^3, and 10^4 (Reynolds numbers $Re = 0.1$, 1, and 10). Although chemical etching is being emphasized, the results of this study are not limited to the etching problem but may be applied to, for example, electrodeposition through masks [11], or other natural and forced convection problems in open cavities. This study considered cavities of a fixed shape as a prelude to studying the effect of natural convection on the shape evolution of cavities.

2. MATHEMATICAL FORMULATION

2.1. *Natural convection system*

A schematic of the free convection system is shown in Fig. 3. A solid film is partially protected by a resist mask having thickness h. The mask forms a rectangular cavity of width $2L$ in the unprotected area of the film. The third dimension (along z) of the cavity was assumed long and therefore a two-dimensional system was considered. The etching solution reacts selectively with the exposed film without attacking the resist mask. Etching takes place under the influence of an acceleration field as shown in Fig. 3. The film dissolution products enter the solution altering the local solution density. This in turn induces convective flow patterns, first within the cavity and later in the near-cavity outside region. Such convective flow patterns affect the rate of mass transport to and from the reactive surface. The dissolution rate is assumed to be controlled by the mass transport of reaction products away from the surface. Hence the product concentration on the film surface is taken equal to the product saturation concentration in the etching solution. Our purpose is to compute the time-dependent local and spatially-averaged mass transfer rate for different cavity aspect ratios A $(=h/2L)$ and Rayleigh numbers. As time progresses and the film dissolves, surface Γ_1 recedes altering the cavity shape and dimensions. In the present work we are interested in the initial stages of dissolution when the cavity dimensions are still essentially unaffected by the dissolution process. The effect of natural convection on the shape evolution of the cavity will be reported elsewhere.

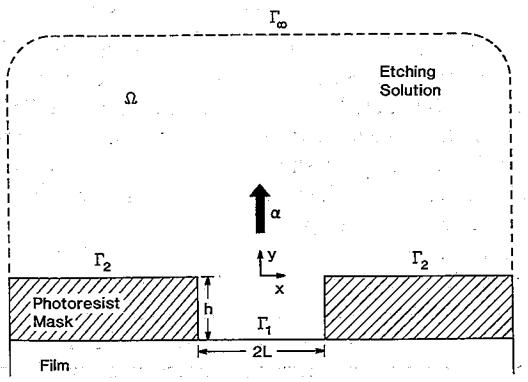

FIG. 3. Schematic of the natural convection system. The acceleration field α is applied in the y-direction.

The fluid was assumed incompressible and Newtonian, and the system was assumed isothermal with constant physical properties except for the solution density. The usual Boussinesq approximation was applied, assuming a constant density in all terms except the body-force term of the Navier–Stokes equations. The solution density was assumed to depend on the concentration of the reaction product according to the following equation of state:

$$\rho = \rho_\infty[1+\beta(c-c_\infty)]. \tag{1}$$

Using the above assumptions the governing equations are written as

$$\frac{\partial \mathbf{u}}{\partial t}+\mathbf{u}\cdot\nabla\mathbf{u} = -\frac{1}{\rho_\infty}\nabla p+\nu\nabla^2\mathbf{u}+\frac{\rho}{\rho_\infty}\alpha \quad \text{in } \Omega \tag{2}$$

$$\nabla\cdot\mathbf{u} = 0 \quad \text{in } \Omega \tag{3}$$

$$\frac{\partial c}{\partial t}+\mathbf{u}\cdot\nabla c = D\nabla^2 c \quad \text{in } \Omega. \tag{4}$$

The governing equations are rendered dimensionless by defining

$$(X, Y) = \frac{1}{L}(x, y), \quad T = \frac{tD}{L^2} \tag{5}$$

$$\mathbf{U} = \frac{L}{D}\mathbf{u}, \quad P = \frac{(p-\rho_\infty\alpha y)L^2}{\mu D} \tag{6}$$

$$C = \frac{c-c_\infty}{c_{\text{sat}}-c_\infty} \tag{7}$$

$$Sc = \frac{\nu}{D}, \quad Ra = \frac{\alpha\beta(c_{\text{sat}}-c_\infty)L^3}{D\nu}. \tag{8}$$

The dimensionless form of the governing equations is

$$\frac{1}{Sc}\left(\frac{\partial \mathbf{U}}{\partial T}+\mathbf{U}\cdot\nabla\mathbf{U}\right) = -\nabla P+\nabla^2\mathbf{U}+Ra\,C\mathbf{j} \quad \text{in } \Omega \tag{9}$$

$$\nabla\cdot\mathbf{U} = 0 \quad \text{in } \Omega \tag{10}$$

$$\frac{\partial C}{\partial T}+\mathbf{U}\cdot\nabla C = \nabla^2 C \quad \text{in } \Omega. \tag{11}$$

The corresponding boundary and initial conditions are

$$\frac{\partial \mathbf{U}}{\partial n} = 0, \quad C = 0 \quad \text{on } \Gamma_\infty \tag{12}$$

$$\mathbf{U} = \mathbf{0}, \quad \frac{\partial C}{\partial n} = 0 \quad \text{on } \Gamma_2 \tag{13}$$

$$\mathbf{U} = \mathbf{0}, \quad C = 1 \quad \text{on } \Gamma_1 \tag{14}$$

$$\mathbf{U} = \mathbf{0}, \quad C = 0 \text{ in } \Omega \text{ at } T = 0 \tag{15}$$

where $\partial/\partial n$ denotes the gradient in the direction of the outward normal to the boundary.

Boundary condition equation (12) implies that the product concentration far from the reacting surface remains equal to c_∞. Boundary condition equation

(13) implies that the product does not react with or penetrate into the mask. The cavity halfwidth L was used as the characteristic length to define the Rayleigh number, although the cavity depth h may be a more appropriate scale. The reason for this choice was that the work presented here is the first step towards studying the effect of natural convection on the shape evolution of cavities, in which case the cavity depth will be a time-varying quantity.

The main parameters of the problem are the Schmidt number Sc, the Rayleigh number Ra, and the cavity aspect ratio A. The dimensionless local mass transfer rate was expressed as a local Sherwood number

$$Sh_x = \frac{k_x L}{D} = \frac{\partial C}{\partial n}. \tag{16}$$

The average Sherwood number along the reactive surface was defined as

$$Sh_{av} = \int_{\Gamma_1} Sh_x \, d\Gamma \Big/ \left(\int_{\Gamma_1} d\Gamma \right). \tag{17}$$

In the extreme case of $Ra = 0$, there is no convective motion, and mass transfer occurs by diffusion alone.

2.2. *Forced convection system*

The case of purely forced convection was examined as well in order to compare the mass transfer results to the natural convection case. The forced convection system is shown in Fig. 4. The system is identical to that of Fig. 3 except that the acceleration field is absent, and that a shear flow prevails far from the cavity. The same governing equations apply as before (equations (9)–(11)) with $Ra = 0$. In this case the relevant parameters are the cavity aspect ratio, the Peclet number defined by equation (18) below, and the Reynolds number $Re = Pe/Sc$

$$Pe = \frac{u_c L}{D}. \tag{18}$$

The boundary and initial conditions appropriate for the forced convection system are [12, 15]

$$\mathbf{U} = \mathbf{0}, \quad C = 1 \quad \text{on} \quad \Gamma_1 \tag{19}$$

$$\frac{\partial U_x}{\partial n} = U_y = 0, \quad C = 0 \quad \text{on} \quad \Gamma_2 \tag{20}$$

$$U_x = \text{constant}, \quad U_y = 0, \quad \frac{\partial C}{\partial n} = 0 \quad \text{on} \quad \Gamma_3 \tag{21}$$

$$\frac{\partial U_x}{\partial n} = U_y = 0, \quad \frac{\partial C}{\partial n} = 0 \quad \text{on} \quad \Gamma_4 \tag{22}$$

$$\mathbf{U} = \mathbf{U}_0, \quad \frac{\partial C}{\partial n} = 0 \quad \text{on} \quad \Gamma_5 \tag{23}$$

$$\mathbf{U} = \mathbf{0}, \quad C = 0 \quad \text{in} \quad \Omega \quad \text{at} \quad T = 0. \tag{24}$$

The Peclet number does not appear explicitly in the governing equations or boundary conditions. However, Pe is directly related to the applied shear rate and therefore to the value of U_x on boundary Γ_3 (boundary condition equation (21)). The relation between Pe and U_x is shown in Table 1. The effect of forced convection on the shape evolution of open cavities during chemical etching was examined in an earlier work [15].

Table 1. Dependence of U_x along boundary Γ_3 (Fig. 4), and of Sherwood number on Peclet number and cavity aspect ratio

Cavity aspect ratio	Peclet number	U_x on Γ_3	Average Sherwood number
1:4	10^2	2.457×10^3	2.463
	10^3	2.460×10^4	4.731
	10^4	2.607×10^5	10.96
1:1	10^2	2.220×10^3	1.071
	10^3	2.222×10^4	2.534
	10^4	2.328×10^5	5.904
2:1	10^2	2.216×10^3	0.3746
	10^3	2.218×10^4	0.5404
	10^4	2.324×10^5	0.8378

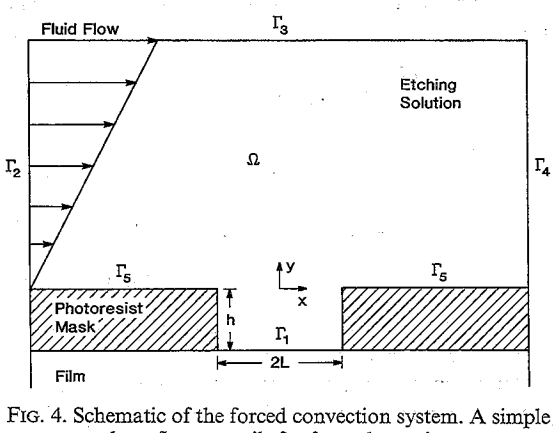

FIG. 4. Schematic of the forced convection system. A simple shear flow prevails far from the cavity.

3. METHOD OF SOLUTION

The solution to the governing equations (9)–(11) subject to the associated boundary conditions (12)–(15) was obtained by using the finite element method. The finite element mesh used for the case of a cavity aspect ratio $A = 1$ is shown in Fig. 5. The mesh was made finer around the mouth of the cavity and within the cavity where steeper concentration gradients are expected. Because the physical domain is unbounded, a problem arises regarding the size of the computational domain, more specifically the location of boundary Γ_∞. Various methods have been proposed to overcome the difficulty associated with an unbounded domain [16–18]. One approach is to position Γ_∞ far from the cavity mouth, so that conditions

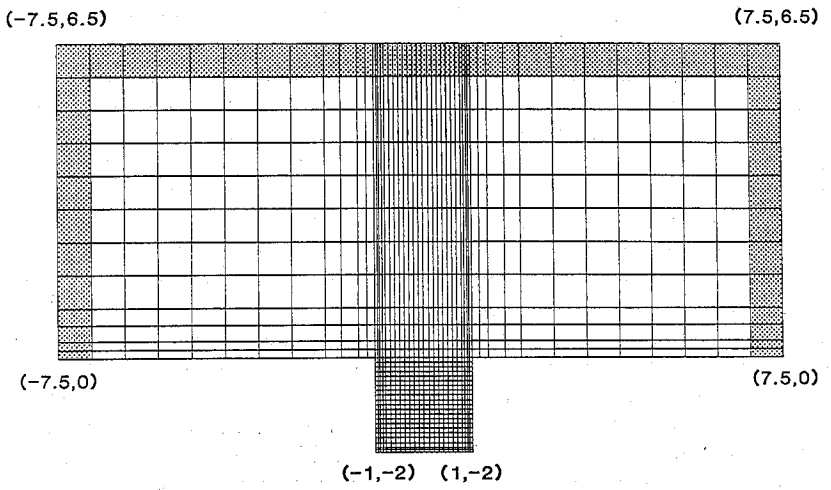

FIG. 5. The finite element mesh used for a 1 : 1 cavity. The dotted elements are mapped infinite elements; the rest are normal finite elements.

near the cavity are not affected by the exact location of the boundary. This approach may result in an unnecessarily large computational domain and hence more CPU time to obtain the solution. Another method is adopted in this work, namely the 'mapped infinite element' method [19, 20]. This method is particularly attractive when used in combination with conventional elements. The elements of the outermost layer in Fig. 5 (dotted area) are mapped infinite elements. The rest are conventional bilinear quadrilateral elements. The total number of elements and nodal points used in Fig. 5 are 1080 and 1162, respectively.

The velocity and concentration fields in the computational domain were obtained by using the penalty function formulation and the Streamline Upwind/Petrov Galerkin (SU/PG) finite element method [21, 22]. Time integration was performed using an implicit predictor–multicorrector scheme [23] with variable time step. A fixed time step may be used as long as stability is assured. However, the fixed time step method may not be as cost effective. For example, a small time step may be required to accurately track the transient behavior of the system during a particular time period, whereas a much larger time step may be adequate for a different time period. In such cases, a variable time step is more effective. The variable time step algorithm used in the present work is similar to that used by Bailey [24].

The transient solution to the two-dimensional problem was obtained in a sequential manner by decoupling the velocity and concentration fields [25, 26]. At time T^n, the velocity field $\mathbf{U}^n$ and the concentration field C^n were known. Here superscript n denotes the nth time step and $T^0 = 0$. Then $\mathbf{U}^{n+1}$ and C^{n+1} were obtained through the following substeps.

(1) With C^n known, $\mathbf{U}^{n+1}$ was calculated from equations (9) and (10) and the associated boundary conditions with an implicit predictor–multicorrector algorithm. If more than five iterations were needed in the corrector step to obtain $\mathbf{U}^{n+1}$, the time step was halved and calculations returned to the predictor step.

(2) With $\mathbf{U}^{n+1}$ known from substep 1 above, C^{n+1} was calculated from equation (11) and the associated boundary conditions with an implicit predictor–multicorrector algorithm.

(3) The Euclidean norm V^{n+1} of $\mathbf{U}^{n+1}$, and in turn the quantity ε was calculated by

$$\varepsilon = \frac{|V^{n+1} - V^n|}{V^{n+1}}. \tag{25}$$

If $\varepsilon < 0.01$, the time step was doubled. If $\varepsilon > 0.1$ the time step was halved. If $0.01 \leqslant \varepsilon \leqslant 0.1$ the time step was not changed. A procedure identical to the one described above (substeps 1–3) was then used to obtain $\mathbf{U}^{n+2}$ and C^{n+2}. Calculations were performed on a CRAY X-MP supercomputer.

In the case of forced convection there is no need to use infinite elements since the concentration boundary layer is always confined near the wall, for the parameter values used. In this case, the position of boundaries Γ_2, Γ_3, and Γ_4 was chosen at $X = -5$, $Y = 4$, and $X = 5$, respectively. Numerical experiments revealed that the results were not affected by positioning boundaries Γ_2, Γ_3, and Γ_4 further away from the cavity mouth. Only the steady-state solution was computed for the forced convection system. The velocity field was obtained by using the penalty function formulation and Newton–Raphson iteration [21]. The velocity field was subsequently used to calculate the concentration field by the SU/PG method.

4. RESULTS AND DISCUSSION

For the natural convection system, results are presented in terms of time-dependent local and spatially-averaged Sherwood numbers for different cavity aspect ratios and Rayleigh numbers. For the forced

convection system results are shown in terms of the steady-state local Sherwood number for different cavity aspect ratios and Peclet numbers. Velocity vector plots and iso-concentration contour plots are used to depict the flow and concentration fields, respectively. All the results shown below were obtained for a Schmidt number $Sc = 10^3$.

Before any further calculations were made, the accuracy of the natural convection numerical code used in the present work was tested by comparing with the solution of natural convection in enclosed cavities given by Taylor and Ijam [2]. The case of unity cavity aspect ratio with Prandtl number $Pr = 10^3$ and $Ra = 10^5$ was chosen for comparison. Results on the temperature and velocity profiles at the cavity mid-height agreed to within 5%. The accuracy of the forced convection code has been verified previously [15].

4.1. *Natural convection system*

Figure 6 shows the time-dependent spatially-averaged Sherwood number for the 1 : 4 cavity and for different Rayleigh numbers. At early times, mass transfer is due to diffusion alone and does not depend on the value of *Ra*. After a certain time, which depends on the value of *Ra*, convective instability sets in and the mass transfer rate increases over the diffusion rate. As *Ra* increases, the instability occurs earlier and the mass transfer rate increases. For low values of *Ra*, the mass transfer enhancement is relatively small and a steady state may be obtained. For higher values of *Ra* (e.g. for $Ra = 10^4$) oscillations in the mass transfer rate are observed. Similar oscillations were observed by Ettefagh and Vafai [5] who studied natural convection in open cavities with a porous medium.

Figure 7 shows the concentration and flow fields for the 1 : 4 cavity, for $Ra = 10^5$, and at four different times which are marked by crosses on the corresponding curve of Fig. 6. At early times, the concentration and flow fields are symmetric with respect to the $X = 0$ axis (Fig. 7(a)). One observes the formation of a primary plume along the axis of symmetry

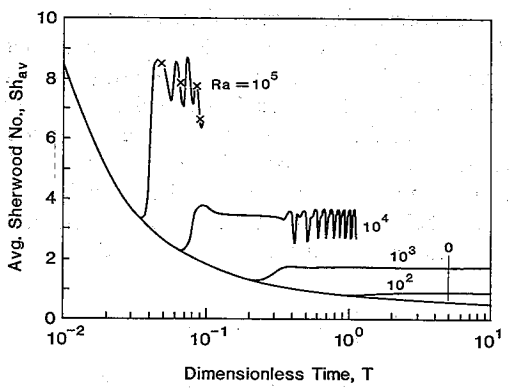

FIG. 6. Spatially-averaged Sherwood number as a function of time for the 1 : 4 cavity and with the Rayleigh number as a parameter.

by which denser solution flows out of the cavity causing 'fresh' solution to flow into the cavity. This incoming flow drives two eddies which fill a large fraction of the cavity volume. The outcoming plume creates, by viscous drag, an almost horizontal flow in the near-cavity outside region, which turns upwards further from the cavity. In addition to the primary plume, two secondary plumes are formed near the corners of the cavity mouth. At later times, symmetry breaking is observed (Fig. 7(b)) which becomes even more pronounced at a still later time (Figs. 7(c) and (d)). Asymmetric flow patterns in an otherwise symmetric two-dimensional vapor-phase epitaxy reactor were recently reported by Weber *et al.* [27]. The authors also presented a bifurcation diagram showing the transition from symmetric to asymmetric flows.

Figure 8 shows the local Sherwood number distribution along the reactive surface for the same times as in Fig. 7. The mass transfer rate is minimum at the corners where the mask meets the reactive surface. This implies that the mask 'undercut' would be smaller than the etched depth, yielding an etch profile which is not isotropic. Etch anisotropy is important especially when deep etching is desired. At early times, a local minimum in mass transfer rate is observed at or near the middle of the active surface. This local minimum is caused by the plume of denser solution flowing out of the cavity. The mass transfer rate distribution becomes less nonuniform when the primary plume shifts to the corner of the cavity mouth (see also Figs. 7(c) and (d)). The mass transfer rate distribution can also be deduced from the concentration contour plots (Fig. 7), in which the spacing between the contours is an indication of the local mass transfer rate.

Figure 9 illustrates the spatially-averaged Sherwood number as a function of time for the 1 : 1 cavity, with *Ra* as a parameter. The same general qualitative features are observed as for the 1 : 4 cavity. However, for a given value of *Ra*, convective instability sets in at a later time as compared to the 1 : 4 cavity. This is a manifestation of the stabilizing effect of the sidewalls. Furthermore, the mass transfer rate is lower for the higher aspect ratio cavity.

Representative concentration and flow fields for the 1 : 1 cavity are shown in Fig. 10 for $Ra = 10^4$, and for the times marked by crosses on the corresponding curve of Fig. 9. As for the 1 : 4 cavity (Fig. 7), symmetry prevails at early times and a plume of denser solution forms. However, the two eddies which occupied a large fraction of the 1 : 4 cavity (Fig. 7(a)) are much smaller in the case of the 1 : 1 cavity (Fig. 10(a)). These eddies are at the corner where the mask meets the reactive surface and cannot be seen on the scale used for the vector plot of Fig. 10(a). Symmetry breaking occurs at later times (Fig. 10(b)), and the asymmetry becomes more pronounced at still later times (Figs. 10(c) and (d)). In the latter case, an eddy occupies a large portion of the cavity volume and this eddy oscillates back and forth within the cavity (Figs. 10(c) and (d)).

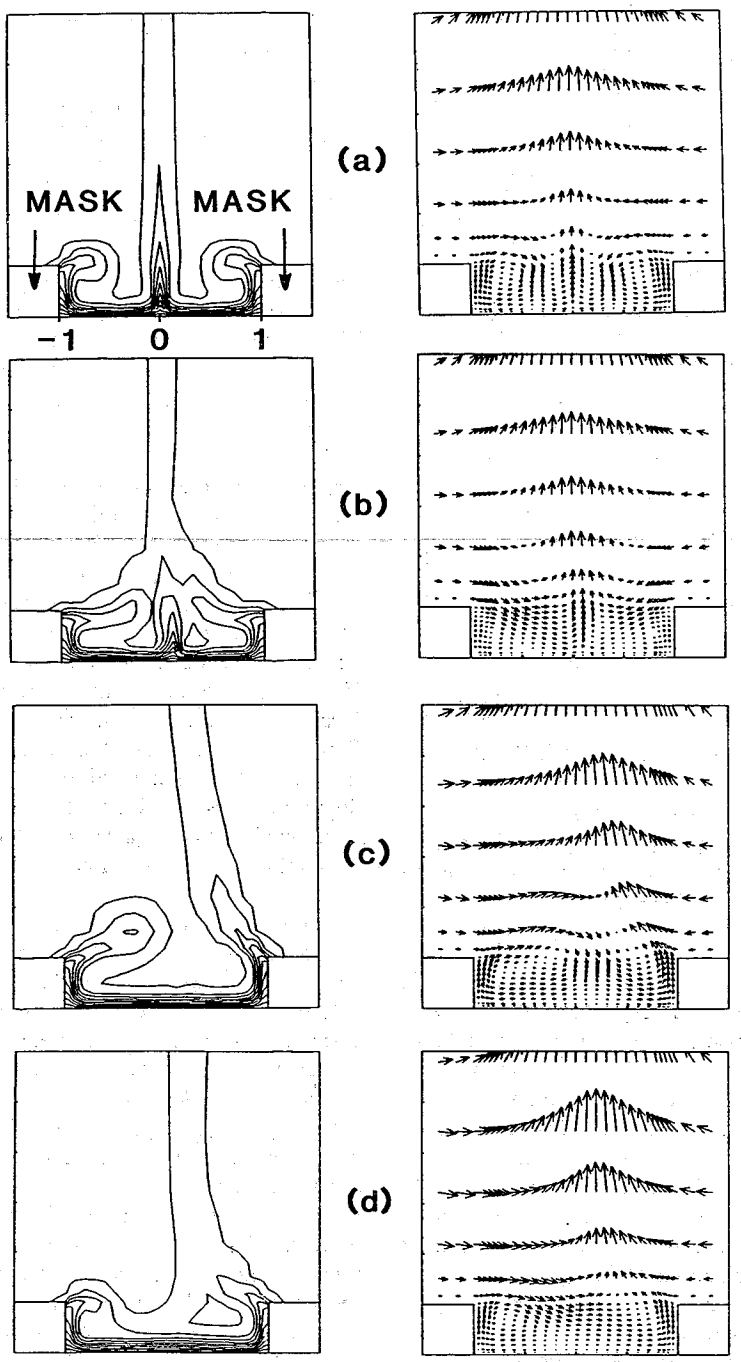

FIG. 7. Concentration contour plot (left) and velocity vector plot (right) at different times for a 1 : 4 cavity, and for a Rayleigh number $Ra = 10^5$. The outermost contour corresponds to $C = 0.01$. The bottom of the cavity corresponds to $C = 1$. Linear interpolation applies for the contours between. Dimensionless times are (a) $T = 4.854 \times 10^{-2}$, (b) $T = 6.564 \times 10^{-2}$, (c) $T = 8.525 \times 10^{-2}$, and (d) $T = 9.064 \times 10^{-2}$.

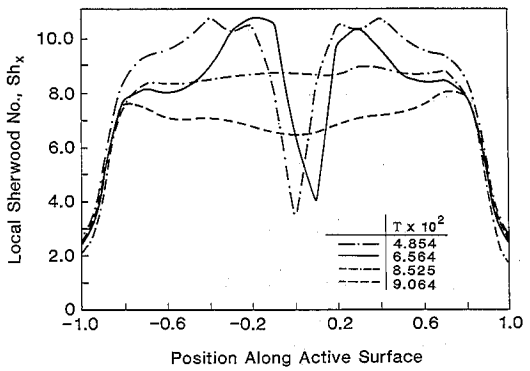

FIG. 8. Local Sherwood number distribution along the active surface at different times for a 1 : 4 cavity and for a Rayleigh number $Ra = 10^5$.

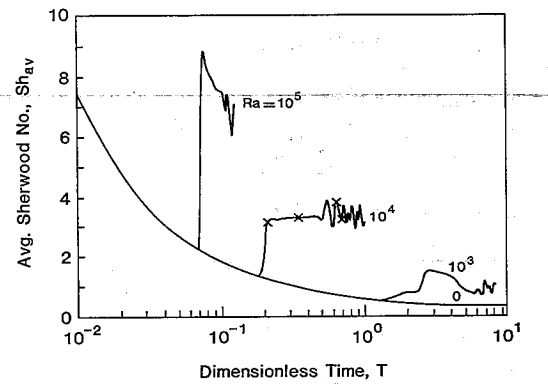

FIG. 9. Spatially-averaged Sherwood number as a function of time for the 1 : 1 cavity and with the Rayleigh number as a parameter.

The local mass transfer distribution is shown in Fig. 11 for the same times as in Fig. 10. At early times, a local minimum appears at or around the midpoint of the active surface. As in Fig. 8, this minimum is associated with the formation of a plume. At later times, the plume shifts to the corners of the cavity mouth and the mass transfer rate is less non-uniform. The broad maximum in mass transfer rate at later times is in the area where an eddy encounters the cavity bottom. Since the eddy oscillates, the maximum in mass transfer oscillates as well.

Figure 12 shows the spatially-averaged Sherwood number as a function of time for the 2 : 1 cavity and for different Rayleigh numbers. One observes the same general qualitative features as for the 1 : 1 cavity (Fig. 9). However, the values of *Sh* are generally lower for the 2 : 1 cavity, although the difference is not as pronounced as when comparing the 1 : 1 cavity to the 1 : 4 cavity. The concentration and velocity vector plots for $Ra = 10^5$ and at four different times are shown in Fig. 13. Similar features are noticed as in Fig. 10, i.e. the formation of a symmetric plume at early times, symmetry breaking and oscillatory behavior at later times. The flow patterns inside the cavity are very complex. The local mass transfer distribution for the 2 : 1 cavity exhibited the same features as for the 1 : 1 cavity (Fig. 11).

4.2. *Forced convection system*

Only the steady-state results are shown for the forced convection system. Table 1 shows the relationship between the Peclet number (as defined by equation (18) and U_x (or equivalently the shear rate) for different cavity aspect ratios. In all cases fluid entered the cavity from the left (Fig. 4). Figures 14(a) and (b) show the concentration contour plot and the velocity vector plot, for the 1 : 4 cavity with $Pe = 10^3$ ($Re = 1$). The external flow penetrates the cavity washing away the reaction products. The fluid velocity is relatively low in the corner regions of the cavity bottom where eddies form. These eddies cannot be resolved on the scale used for the velocity vector plot. The flow patterns are similar for $Re = 0.1$ and 10, but the velocities differ. The local Sherwood number for the 1 : 4 cavity is shown in Fig. 14(c) for three values of *Pe*. As expected, the average *Sh* increases with increasing *Pe* (see also Table 1). The mass transfer rate is relatively high around the region where the external flow first encounters the cavity bottom (around $X = -0.4$, see Fig. 14(a)). The mass transfer rate passes through a local minimum around the region where the external flow turns away from the cavity bottom (around $X = 0.5$). The maxima and minima of the mass transfer rate can also be deduced from the concentration contour plot (Fig. 14(a)), where the spacing between the contours is an indication of the local mass transfer rate.

Figure 15 shows the concentration contour plots for the 1 : 1 cavity and for three different values of *Pe* ($Pe = 10^2$, 10^3, 10^4). In the 1 : 1 cavity case, the external flow can no longer penetrate the cavity. Instead, a large recirculating eddy forms which fills the cavity volume. The formation of a mass transfer boundary layer along the active surface is clearly seen, especially for the higher values of *Pe*. The boundary layer becomes thinner as *Pe* increases. The concentration is nearly uniform in the cavity core outside the boundary layer. Another 'boundary layer' is seen to form along the cavity mouth, preventing effective communication between the external flow and the interior of the cavity. This communication can be restored in the presence of natural convection (Fig. 10).

Figure 16 shows the local Sherwood number as a function of position along the active surface for the 1 : 1 cavity and for different values of *Pe*. The rate of mass transfer increases and its distribution becomes less uniform as *Pe* increases. The mass transfer rate attains a maximum between the center and the right corner of the cavity bottom. This maximum is associated with a clockwise eddy filling almost the entire cavity volume. The maximum occurs at the point where the eddy first encounters the cavity bottom.

FIG. cavity of the

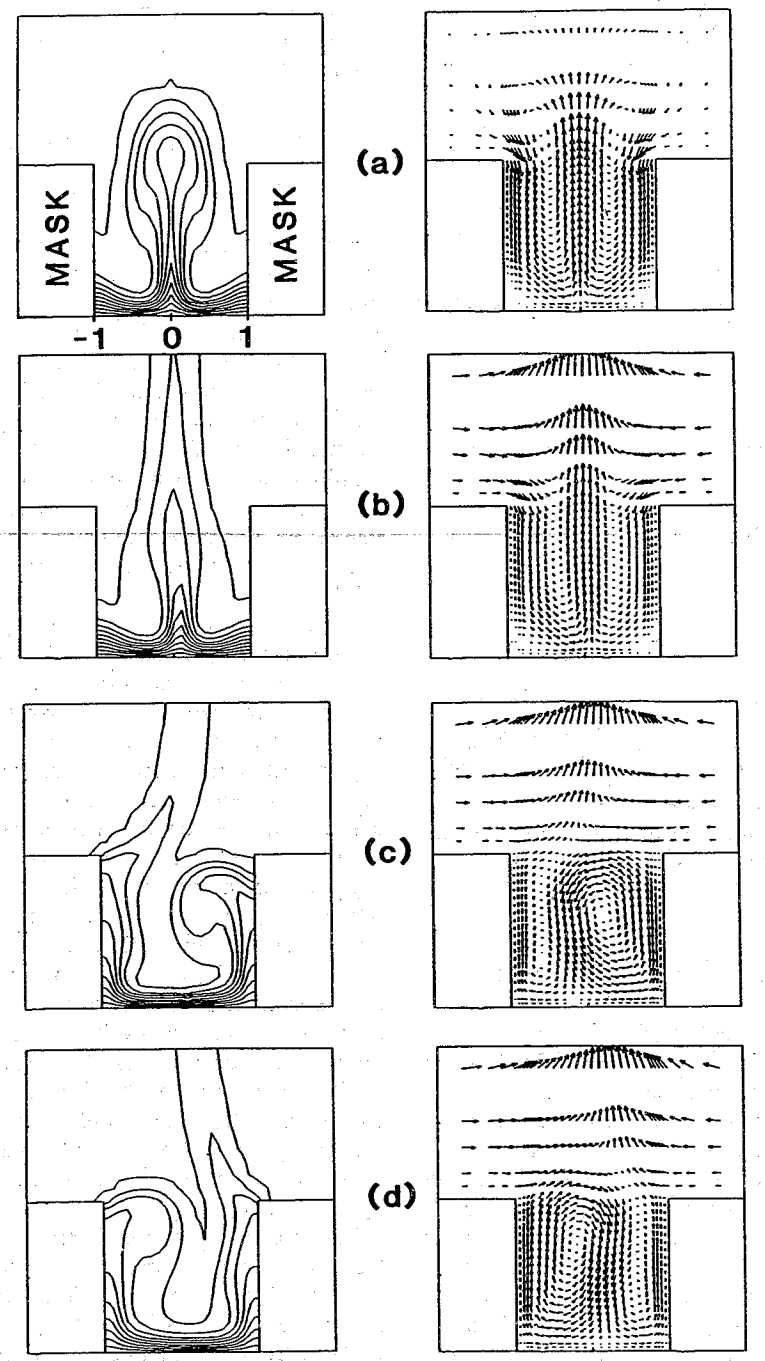

FIG. 10. Concentration contour plot (left) and velocity vector plot (right) at different times for a 1:1 cavity, and for a Rayleigh number $Ra = 10^4$. The outermost contour corresponds to $C = 0.01$. The bottom of the cavity corresponds to $C = 1$. Linear interpolation applies for the contours between. Dimensionless times are (a) $T = 0.2113$, (b) $T = 0.3472$, (c) $T = 0.6372$, and (d) $T = 0.6922$.

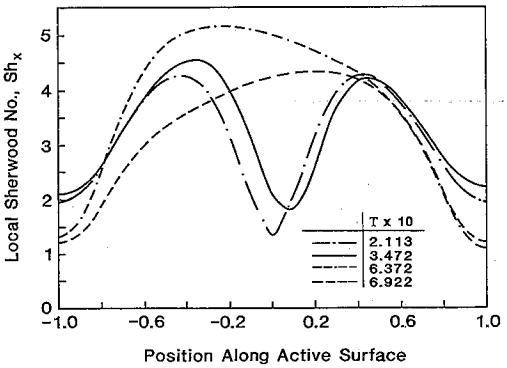

FIG. 11. Local Sherwood number distribution along the active surface at different times for a 1:1 cavity and for a Rayleigh number $Ra = 10^4$.

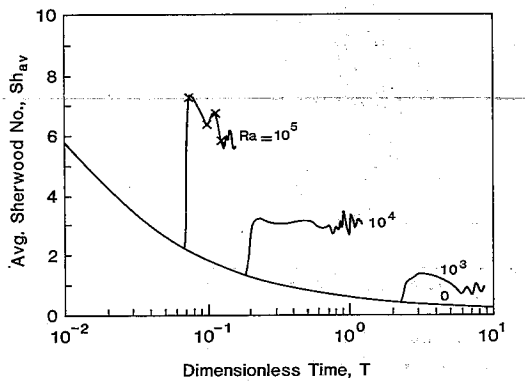

FIG. 12. Spatially-averaged Sherwood number as a function of time for a 2:1 cavity and with the Rayleigh number as a parameter.

The maximum becomes more pronounced as Pe increases.

The concentration contour plots for the 2:1 cavity are shown in Fig. 17 for three values of Pe. The flow field in the 2:1 cavity consists of a main clockwise eddy driven by the external flow, and a secondary counter-clockwise eddy underneath the first. The fluid motion is very weak in the secondary eddy and mass transfer in this region is mainly by diffusion, especially at low values of Pe. Hence the concentration contour plots deeper in the cavity are nearly parallel to the reactive surface. The corresponding local Sh distribution is shown in Fig. 18. Mass transfer is nearly uniform for $Pe = 10^2$ and 10^3. However, mass transfer attains a maximum for $Pe = 10^4$. The maximum is in the region where the secondary eddy first encounters the cavity bottom.

The steady-state spatially-averaged Sherwood number results for the forced convection system are summarized in Table 1 (last column). By comparing with the corresponding values of the natural convection system (Figs. 6, 9, and 12), one observes that natural convection is particularly advantageous for enhancing mass transfer in high aspect ratio cavities. For example, for the 2:1 cavity and for a comparable magnitude of the fluid velocity at the center of the cavity mouth, natural convection yields a mass transfer rate one order of magnitude higher than forced convection. This is of great importance in etching of deep cavities.

5. SUMMARY AND CONCLUSIONS

The time-dependent mass transfer by natural convection in two-dimensional open cavities was studied for a Schmidt number of 10^3. The Streamline Upwind/Petrov Galerkin finite element method with an implicit predictor–multicorrector algorithm was employed. The method of mapped infinite elements was used to treat the unbounded domain. The effect of cavity aspect ratio and of Rayleigh number on the local and spatially-averaged Sherwood number was examined. Forced convection mass transfer calculations were also performed for different cavity aspect ratios and Peclet numbers. Emphasis was placed on a system simulating selective chemical etching of thin solid films in microelectronic device fabrication.

In the natural convection system, plumes of denser solution formed, which caused 'contaminated' solution to flow out of the cavity and 'fresh' solution to flow into the cavity, thereby providing an effective means of mass transport. This was especially true for high aspect ratio (deep) cavities which are difficult to access by other means as, for example, by forced convection. The flow and concentration fields were symmetric at early times. However, symmetry breaking and oscillatory flows, with concomitant oscillations in the mass transfer, were observed at later times. The oscillatory behavior was characterized by complex cellural flow patterns within the cavity. The mass transfer rate distribution was nonuniform along the active surface, and it was, in general, substantially lower at the corners where the inert surface (mask) met the active surface. This fact has implications for the etch anisotropy achievable with the natural convection system. The average mass transfer rate increased with increasing Ra and with decreasing cavity aspect ratio.

Forced convection was effective in enhancing mass transfer in low aspect ratio (shallow) cavities. However, for deep cavities, slow recirculating flows and boundary layers along the cavity mouth prevented effective communication of the external flow with the cavity interior, causing a drastic decrease in mass transfer. The mass transfer rate distribution along the active surface was non-uniform, especially at high Peclet numbers. The average mass transfer rate increased with increasing Peclet number and with decreasing cavity aspect ratio.

When compared to forced convection, natural convection is very attractive for enhancing the mass transfer in deep cavities. For example, for a 2:1 cavity, and for comparable magnitude of the fluid velocity at the

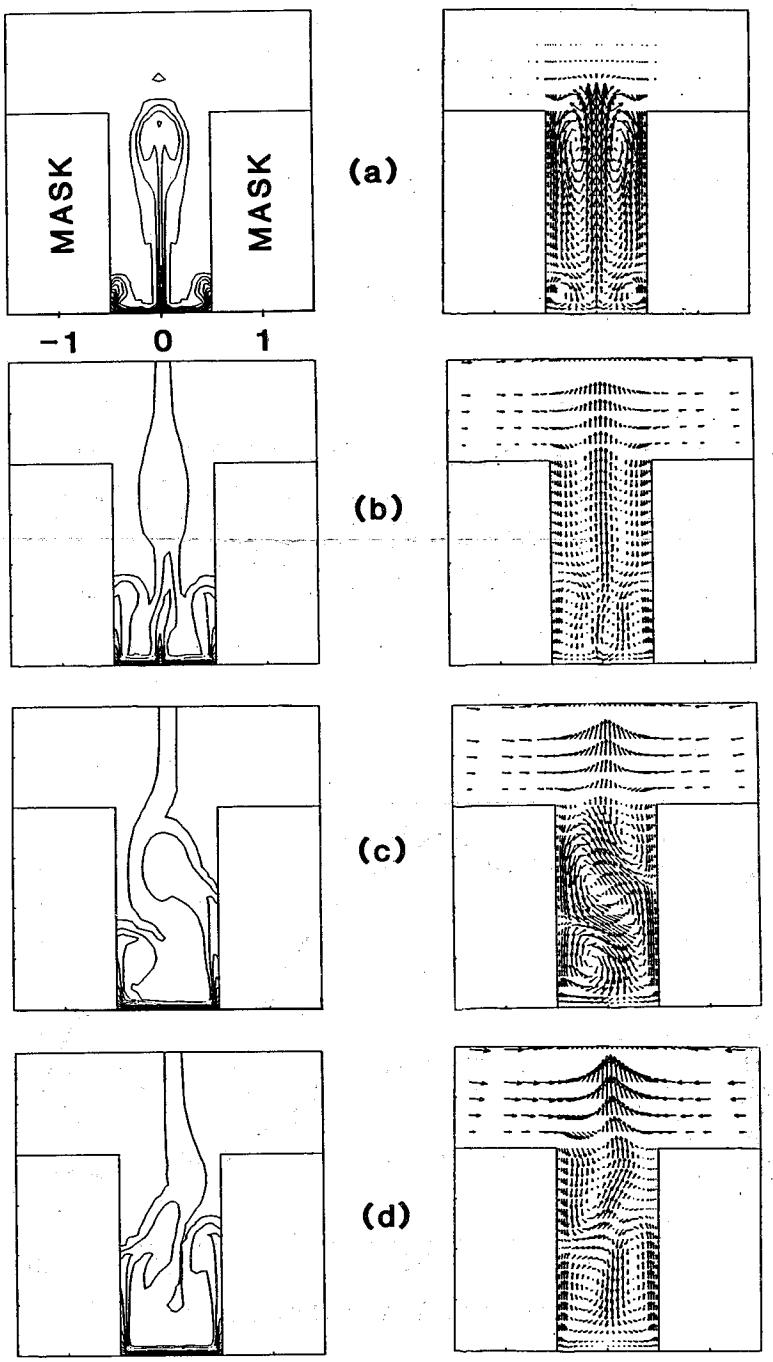

FIG. 13. Concentration contour plot (left) and velocity vector plot (right) at different times for a 2:1 cavity, and for a Rayleigh number $Ra = 10^5$. The outermost contour corresponds to $C = 0.01$. The bottom of the cavity corresponds to $C = 1$. Linear interpolation applies for the contours between. Dimensionless times are (a) $T = 7.520 \times 10^{-2}$, (b) $T = 9.994 \times 10^{-2}$, (c) $T = 1.156 \times 10^{-1}$, and (d) $T = 1.270 \times 10^{-1}$.

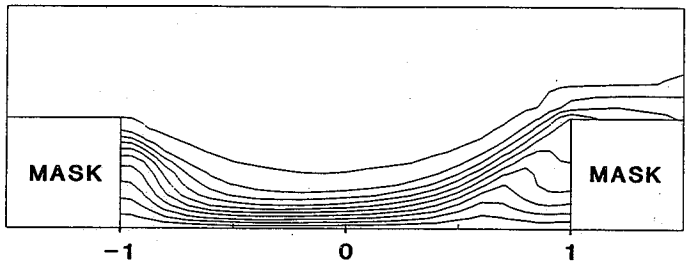

(a)

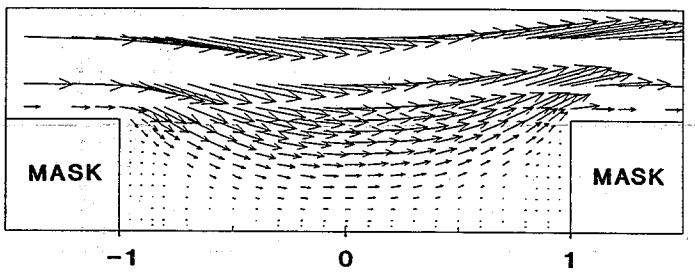

(b)

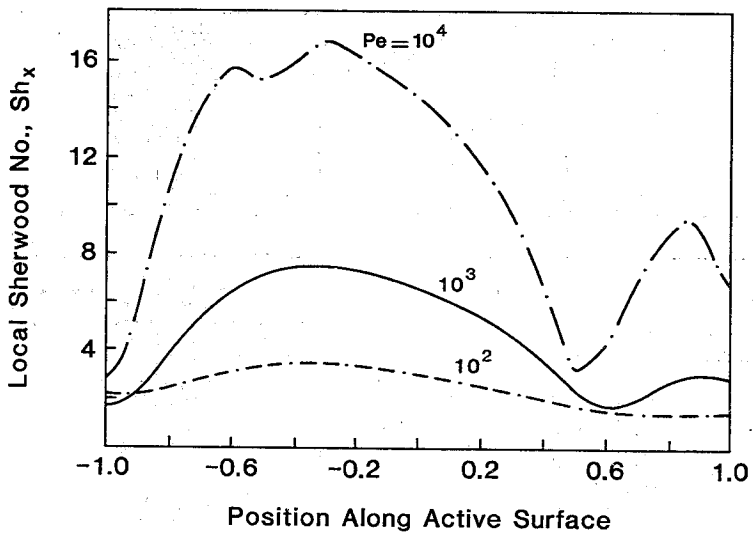

(c)

FIG. 14. Concentration contour plot (a) and velocity vector plot (b) for forced convection over a 1:4 cavity with Peclet number $Pe = 10^3$ (Reynolds number $Re = 1$). The outermost contour corresponds to $C = 0.01$. The bottom of the cavity corresponds to $C = 1$. Linear interpolation applies for the contours between. (c) Local Sherwood number distribution along the active surface for forced convection over a 1:4 cavity and for different Peclet numbers.

FIG. 15. Co
over a 1:
(c) $Pe = 1$
$C = 0.01$. T
Linear in

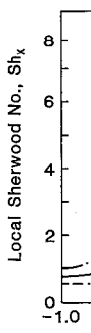

FIG. 16. L
active surfa

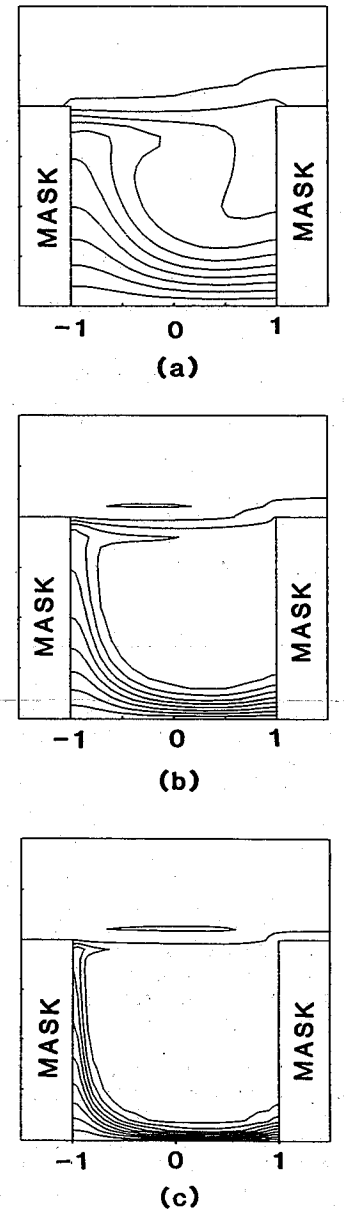

FIG. 15. Concentration contour plot for forced convection over a 1:1 cavity: (a) $Pe = 10^2$, (b) $Pe = 10^3$, and (c) $Pe = 10^4$. The outermost contour corresponds to $C = 0.01$. The bottom of the cavity corresponds to $C = 1$. Linear interpolation applies for the contours between.

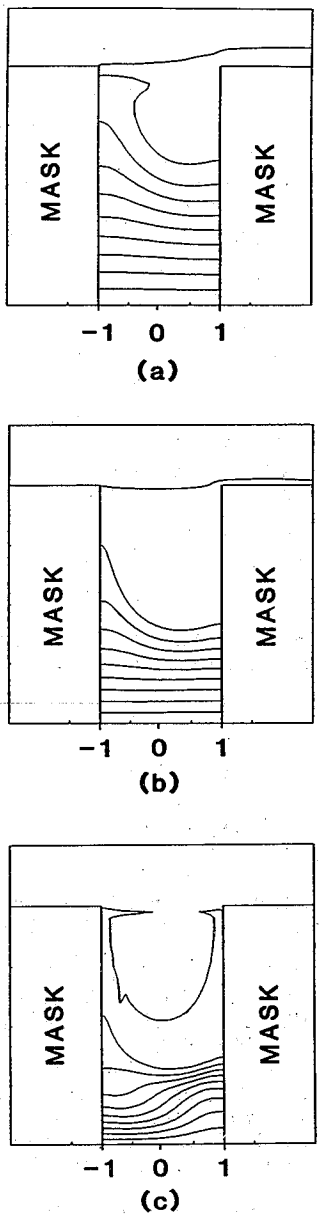

FIG. 17. Concentration contour plot for forced convection over a 2:1 cavity: (a) $Pe = 10^2$, (b) $Pe = 10^3$, (c) $Pe = 10^4$. The outermost contour corresponds to $C = 0.01$. The bottom of the cavity corresponds to $C = 1$. Linear interpolation applies for the contours between.

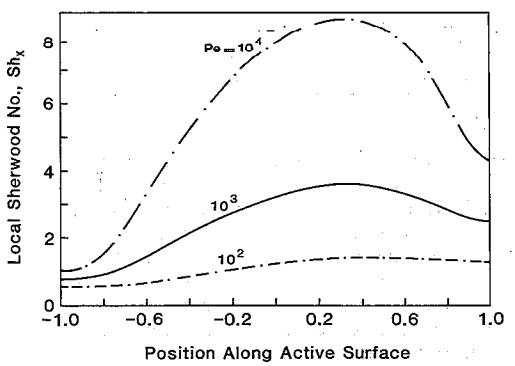

FIG. 16. Local Sherwood number distribution along the active surface for forced convection over a 1:1 cavity and for different Peclet numbers.

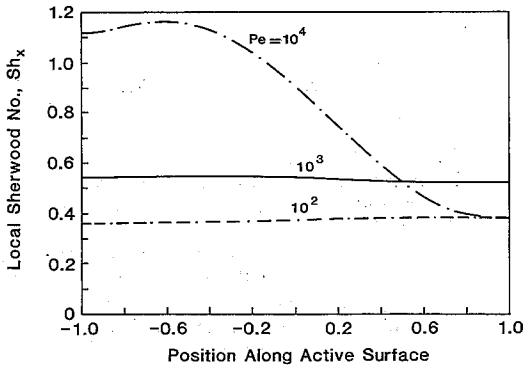

FIG. 18. Local Sherwood number distribution along the active surface for forced convection over a 2:1 cavity and for different Peclet numbers.

center of the cavity mouth, natural convection yielded a mass transfer rate one order of magnitude higher than that of forced convection. Therefore, natural convection may be useful in etching of deep cavities.

The system examined in the present work is only a simplification of practical etching systems. For example, a cavity of invariant shape was considered, although shape evolution occurs during etching [15]. However, the present work was thought to be a logical first step before examining the effect of natural convection on the shape evolution of cavities. Finally it should be noted that, from a practical point of view, natural convection may not be viable for very small geometries due to the strong dependence of Ra on the length scale ($Ra \sim L^3$). Thus, for very small cavities, a very large acceleration field (α) may be needed to exceed the critical value of Ra for convection to set in.

Acknowledgements—We are grateful to Cray Research Inc. for a supercomputer time grant (Mr David Dealy, grant monitor).

REFERENCES

1. Y. Jaluria, *Natural Convection Heat and Mass Transfer*. Pergamon Press, Oxford (1980).
2. C. Taylor and A. Z. Ijam, A finite element numerical solution of natural convection in enclosed cavities, *Comput. Meth. Appl. Mech. Engng* **19,** 429–446 (1979).
3. Y. Yamaguchi, C. J. Chang and R. A. Brown, Multiple buoyancy-driven flows in a vertical cylinder heated from below, *Phil. Trans. R. Soc. Lond.* **A312,** 519–552 (1984).
4. K. R. Kirchartz and H. Oertel, Jr., Three-dimensional thermal cellular convection in rectangular boxes, *J. Fluid Mech.* **192,** 249–286 (1988).
5. J. Ettefagh and K. Vafai, Natural convection in open-ended cavities with a porous obstructing medium, *Int. J. Heat Mass Transfer* **31,** 673–693 (1988).
6. Y. L. Chan and C. L. Tien, Laminar natural convection in shallow open cavities, *J. Heat Transfer* **108,** 305–309 (1986).
7. H. K. Kuiken, Heat or mass transfer from an open cavity, *J. Engng Math.* **12,** 129–155 (1978).
8. R. Alkire and H. Deligianni, The role of mass transfer on anisotropic electrochemical pattern etching, *J. Electrochem. Soc.* **135,** 1093–1100 (1988).
9. J. L. Vossen and W. Kern (Editors), *Thin Film Processes*. Academic Press, New York (1978).
10. R. E. Williams, *Gallium Arsenide Processing Techniques*. Atrech House Inc., Dedham (1984).
11. E. C. Hume, W. M. Deen and R. A. Brown, Mass transfer analysis of electrodeposition through polymeric masks, *J. Electrochem. Soc.* **131,** 1251–1258 (1984).
12. R. C. Alkire, D. B. Reiser and R. L. Sani, Effect of fluid flow on removal of dissolution products from small cavities, *J. Electrochem. Soc.* **131,** 2795–2800 (1984).
13. J. J. L. Higdon, Stokes flow in arbitrary two-dimensional domains: shear flow over ridges and cavities, *J. Fluid Mech.* **159,** 195–226 (1985).
14. H. K. Kuiken and R. P. Tijburg, Centrifugal etching: a promising new tool to achieve deep etching results, *J. Electrochem. Soc.* **130,** 1722–1729 (1983).
15. C. B. Shin and D. J. Economou, Effect of transport and reaction on the shape evolution of cavities during wet chemical etching, *J. Electrochem. Soc.* **136,** 1997–2004 (1989).
16. P. Bettess, More on infinite elements, *Int. J. Numer. Meth. Engng* **15,** 1613–1626 (1980).
17. G. Beer and J. L. Meek, 'Infinite domain' elements, *Int. J. Numer. Meth. Engng* **17,** 43–52 (1981).
18. P. P. Lynn and H. A. Hadid, Infinite elements with $1/r^n$ type decay, *Int. J. Numer. Meth. Engng* **17,** 347–355 (1981).
19. O. C. Zienkiewicz, C. Emson and P. Bettess, A novel boundary infinite element, *Int. J. Numer. Meth. Engng* **19,** 393–404 (1983).
20. J. M. M. C. Marques and D. R. J. Owen, Infinite elements in quasi-static materially nonlinear problems, *Comput. Struct.* **18,** 739–751 (1984).
21. T. J. R. Hughes, W. K. Liu and A. Brooks, Finite element analysis of incompressible viscous flows by the penalty function formulation, *J. Comput. Phys.* **30,** 1–60 (1979).
22. A. N. Brooks and T. J. R. Hughes, Streamline Upwind/Petrov Galerkin formulations for convection dominated flows with particular emphasis on the incompressible Navier–Stokes equations, *Comput. Meth. Appl. Mech. Engng* **32,** 199–259 (1982).
23. T. J. R. Hughes, K. S. Pister and R. L. Taylor, Implicit–explicit finite elements in nonlinear transient analysis, *Comput. Meth. Appl. Mech. Engng* **17/18,** 159–182 (1979).
24. H. E. Bailey, Numerical integration of the equations governing the one-dimensional flow of a chemically reactive gas, *Physics Fluids* **12,** 2292–2300 (1969).
25. J. H. Argyris and J. St. Doltsinis, On the natural formulation and analysis of large deformation coupled thermomechanical problems, *Comput. Meth. Appl. Mech. Engng* **25,** 195–253 (1981).
26. J. H. Argyris, J. St. Doltsinis, P. M. Pimenta and H. Wustenberg, Natural finite element techniques for viscous fluid motion, *Comput. Meth. Appl. Mech. Engng* **45,** 3–55 (1984).
27. C. Weber, C. van Opdorp and M. de Keijser, Modeling of gas-flow patterns in a symmetric vertical vapor-phase-epitaxy reactor allowing asymmetric solutions, *J. Appl. Phys.* **67,** 2109–2118 (1990).

TRANSFERT DE MASSE PAR CONVECTION NATURELLE ET FORCEE DANS DES CAVITES OUVERTES

Résumé—On étudie le transfert variable de masse par convection naturelle dans des cavités ouvertes bidimensionnelles en utilisant la méthode des éléments finis. L'attention est portée sur un système simulant la gravure chimique sélective des films solides minces pour la fabrication des éléments microélectroniques. Des nombres de Sherwood locaux dépendants du temps et moyens dans l'espace sont rapportés pour un nombre de Schmidt de 10^3, des rapports de forme de cavité (profondeur : largeur) de 1 : 4, 1 : 1 et 2 : 1 et pour des nombres de Rayleigh allant jusqu'à 10^5. Les champs d'écoulement et de concentration sont symétriques au début. La symétrie disparait et des écoulements oscillants s'installent ensuite. La formation de panaches se produit à cause de la communication entre la solution externe neuve et la solution usée dans la cavité, spécialement pour des cavités profondes qui sont d'accès difficile. On étudie aussi la convection forcée de masse pour des nombres de Peclet allant jusqu'à 10^4. Les résultats sont importants pour les gravages anisotropes profonds des films minces solides et d'autres procédés connexes.

STOFFÜBERGANG DURCH NATÜRLICHE UND ERZWUNGENE KONVEKTION IN OFFENEN HOHLRÄUMEN

Zusammenfassung—Mit einer Finite-Elemente-Methode wird der zeitabhängige Stofftransport durch natürliche Konvektion in zweidimensionalen offenen Hohlräumen untersucht. Damit soll selektives chemisches Ätzen dünner Schichten simuliert werden, wie es bei der Fertigung im Bereich der Mikroelektronik angewandt wird. Zeitabhängige, örtliche und räumlich gemittelte Sherwood-Zahlen werden für eine Schmidt-Zahl von 10^3, für Seitenverhältnisse des Hohlraums (Tiefe : Breite) von 1 : 4, 1 : 1 und 2 : 1 und für Rayleigh-Zahlen bis 10^5 dargestellt. Strömungs- und Konzentrations-Verteilung sind anfangs symmetrisch, später treten jedoch ein Aufbrechen der Symmetrie und ein Schwingen der Strömung auf. Die Ausbildung von Auftriebsfahnen führt zu einem effektiven Austausch zwischen der äußeren "sauberen" Ätzlösung und der "verschmutzten" Lösung innerhalb des Hohlraums. Dies ist besonders für tiefe Hohlräume wichtig, die sonst schwer zugänglich sind. Es wird auch erzwungene Konvektion für Peclet-Zahlen bis 10^4 untersucht. Im Vergleich zur erzwungenen Konvektion ergibt sich bei natürlicher Konvektion im 2 : 1-Hohlraum eine Erhöhung des Stoffaustausches um eine Größenordnung. Die Ergebnisse sind von großer Bedeutung für tiefe anisotrope Ätzungen dünner Schichten und andere ähnliche Prozesse.

МАССОПЕРЕНОС ЕСТЕСТВЕННОЙ И ВЫНУЖДЕННОЙ КОНВЕКЦИЕЙ В НЕЗАМКНУТЫХ ПОЛОСТЯХ

Аннотация—Методом конечных элементов исследуется нестационарный массоперенос, вызванный естественной конвекцией в двумерных незамкнутых полостях. Особое внимание уделяется системе, моделирующей избирательное химическое травление тонких твердых пленок, применяемое при производстве микроэлектронных элементов. Представлены зависящие от времени локальные и пространственно усредненные значения числа Шервуда для значения числа Шмидта 10^3, отношений сторон полости (глубина : ширина) 1 : 4, 1 : 1 и 2 : 1 и для значений числа Рэлея вплоть до 10^5. На начальной стадии поля скоростей течения и концентраций являются симметричными. Однако на более поздних стадиях происходит нарушение симметрии и возникают колебательные режимы. Образование восходящих струй приводит к эффективному взаимодействию вновь поступающего "свежего" травильного раствора с "загрязненным" раствором, особенно для глтбоких полостей, доступ в которые в противном случае затруднен. Исследуется также массоперенос вынужденной конвекцией при значениях числа Пекле до 10^4. По сравнению со случаем вынужденной конвекции естественноконвективный массоперенос на порядок интенсивней в полости с отношением сторон 2 : 1. Полученные результаты имеют большое значение для глубокого анизотропного травления тонких твердых пленок и других связанных с ним процессов.